

# Chloride penetration in concrete under varying humidity and temperature changes: A numerical study

Liang-yu Tong<sup>a</sup>, Branko Šavija<sup>c</sup>, Mingzhong Zhang<sup>d</sup>, Qing Xiang Xiong<sup>a,e</sup>, Qing-feng Liu<sup>a,b,c\*</sup>

<sup>a</sup> State Key Laboratory of Ocean Engineering, School of Ocean and Civil Engineering, Shanghai Jiao Tong University, Shanghai, China

<sup>b</sup> State Key Laboratory of Subtropical Building and Urban Science, South China University of Technology, Guangzhou, China

<sup>c</sup> Microlab, Faculty of Civil Engineering and Geosciences, Delft University of Technology, Delft, 2628CN, the Netherlands

<sup>d</sup> Department of Civil, Environmental and Geomatic Engineering, University College London, London WC1E 6BT, UK

<sup>e</sup> Shanghai Key Laboratory for Digital Maintenance of Buildings and Infrastructure, Shanghai, China

\* Corresponding Author. Email address: liuqf@sjtu.edu.cn

**Abstract:** When serving in the marine environment, reinforced concrete structures are prone to be attacked by chloride ingress, which generally co-occurs with varying humidity and temperature changes. Therefore, considering the interaction between moisture transport and heat transfer, and their individual and coupling effects on chloride transport, this paper presents a novel numerical modelling framework for chloride penetration in concrete under different environmental conditions. In this framework, a novel thermal conductivity model and temperature-depended chloride binding isotherms are also developed, considering the heterogeneous characteristics of concrete. The proposed model is validated against a series of experimental data. By assuming the cyclic humidity and temperature boundary conditions as trigonometric type, this study further discusses the effect of average value, amplitude value and period length of cyclic environmental changes on the chloride transport in concrete. The results indicate that variation in humidity and temperature averages can alter the peak values of chloride content but have less effect on the chloride penetration depth. However, the increased humidity amplitude could significantly promote both the peaks and the penetration depths due to intensive chloride convection caused by moisture transport. This paper is supposed to provide a better understanding of chloride penetration in concrete under a realistic engineering environment.

**Keywords:** Concrete; Chloride penetration; Wetting-drying; Temperature; Cyclic boundary

1    **1. Introduction**

2       The chloride-induced corrosion problem is recognised as one of the most deleterious factors  
3       causing durability degradation of reinforced concrete (RC) structures served in marine or offshore  
4       regions. The concentration gradient of chloride between the seawater and the internal pore solution  
5       of concrete will lead to the chloride diffusion in concrete cover and finally result in the structure  
6       damage, e.g., the corrosion of embedded rebars, which plays a vital role in the service life  
7       prediction and durability assessment of concrete structures [1, 2]. Besides, due to the diurnal  
8       temperature differences or seasonal variations and dry-wetting cycles, concrete structures are  
9       always exposed to chloride ingress under varying temperatures and humidities conditions [3, 4].  
10      Thus, in this condition, the effect of temperature and humidity changes on chloride penetration  
11      should not be ignored, and the investigation of chloride ingress subjected to an unsaturated non-  
12      isothermal state is of great significance for both structure design and maintenance [5-9].

13      In the past decades, the ingress process of chloride in concrete structures under isothermal and  
14      saturated conditions has been widely studied both experimentally and numerically [10-14].  
15      However, with the temperature and humidity changes, chloride penetration will be affected by the  
16      moisture and heat transfer and become more complex, and has rarely been investigated [15-18].  
17      In the past few years, some studies have considered the effect of temperature on the rates of  
18      chloride and moisture transport during wetting-drying cycles [15, 19-22]. However, in their  
19      studies, the environmental temperature was kept constant for simulations, and the coupling  
20      interaction between moisture and heat transfer was not considered. In recent years, a series of  
21      experimental and analytical studies on the interaction between any two of chloride, moisture and  
22      heat transport have been conducted in Refs. [6, 23-26], but the coupled chloride-moisture-heat  
23      transport was not addressed. Additionally, although it has been widely accepted that the rising  
24      temperature can promote both moisture and chloride transport [8, 23, 27, 28], the interaction  
25      between moisture transport and heat transfer has rarely been studied. Unsaturated concrete can be  
26      regarded as a composite consisting of a solid skeleton and water- and gas-filled pore structures  
27      with different thermal conductivities [29, 30]. Therefore, the moisture transport can change the  
28      water content and distribution, affecting the ions' transport channels and the concrete's thermal  
29      conductivity. The heat transfer, in turn, would influence the moisture transport process. Therefore,

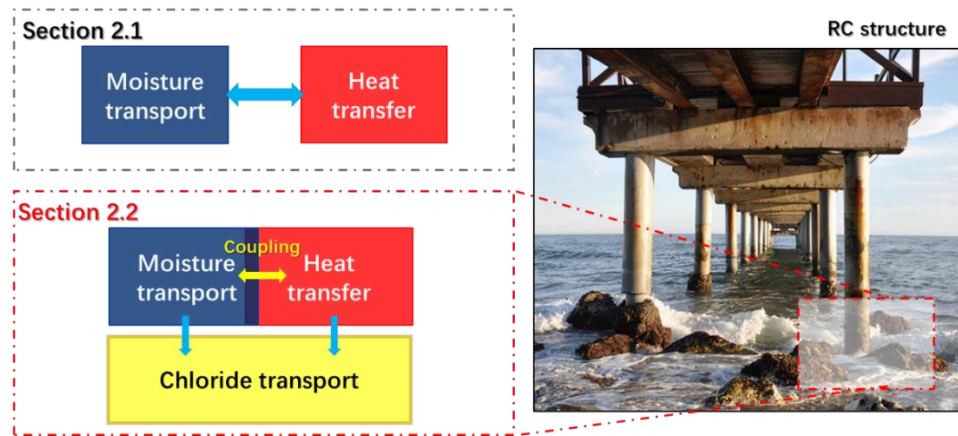
30 more research is required to explore coupled moisture and heat transfer processes and analyse their  
1  
2 coupling effect on chloride transport under varying humidity and temperature changes.  
3  
4

5 It is difficult, if not impossible, to experimentally consider different phenomena during  
6 coupled chloride-moisture-heat transport in concrete structures. Therefore, numerical studies  
7  
8 would offer effective tools for estimating the effects of various parameters on such complex  
9 phenomena [23, 31-33]. Because chloride ions may adhere to the cement matrix of the pore  
10 structure physically and chemically, which decelerates the chloride transport, the effect of chloride  
11 binding must be considered for chloride transport modelling. At present, it has been reported  
12 experimentally that chloride binding capacity would be altered at different temperatures [34, 35].  
13  
14 However, how to consider the different chloride binding capacities at varied temperatures in  
15 chloride transport modelling still needs further research. Moreover, realistic engineering  
16 environments are always diverse, where the temperature, relative humidity, and surface chloride  
17 concentrations often experience cyclical variations [36-39]. Although some existing numerical  
18 models were developed to analyse the chloride transport process subjected to wetting-drying  
19 cycles, the temperature variation was always ignored. To the best of the author's knowledge, the  
20 numerical study on chloride transport in cementitious materials accounting for both cyclically  
21 varied humidity and temperature boundary conditions is still lacking.  
22  
23

24 In this study, a numerical model was proposed to investigate chloride transport under varying  
25 humidity and temperature changes. Transport properties of concrete, including chloride diffusion  
26 coefficient, moisture diffusion coefficient and thermal conductivity, are determined based on the  
27 heterogeneous characteristics of concrete, which are related to changed humidity and  
28 temperatures. The intrinsic interaction of moisture transport and heat transfer, as well as their  
29 individual and coupling effects on the chloride ingress, are comprehensively analysed and  
30 discussed. The chloride distributions, including free and bound chlorides, in cementitious materials  
31 under various environmental conditions are predicted and validated with experimental data from  
32 the literature. In addition, the effects of the average value, amplitude value and period length of  
33 cyclic environmental humidity and temperature changes on the chloride transport process in  
34 concrete are discussed quantitatively.  
35  
36

59 **2. Model setup**

1 To model the coupled processes of chloride transport, moisture and heat transfer, two  
 2 procedures will be carried out in this section, as shown in **Fig. 1**. Firstly, coupled moisture and  
 3 heat transfer, as well as their interaction relationship, will be analysed in Section 2.1. Then,  
 4 considering the individual effect of moisture and heat transfer and their coupled effect on chloride  
 5 penetration, the chloride transport process under varying humidity and temperature changes will  
 6 be modelled in Section 2.2.  
 7  
 8  
 9  
 10  
 11  
 12



21 Fig. 1 Illustration of individual and coupled transport processes.  
 22  
 23  
 24  
 25  
 26  
 27  
 28  
 29

30 **2.1 Coupled moisture and heat transfer**

31 **2.1.1 Governing equation**

32  
 33 Moisture serves as the transport medium for chloride ions. In unsaturated concrete, moisture  
 34 transport in both gaseous and liquid water states, which are driven by the vapour pressure  
 35 difference and capillary pressure differences, respectively. The moisture flux  $J$  is proportional to  
 36  
 37  
 38  
 39  
 40  
 41  
 42  
 43  
 44

$$J = -(K_l \nabla P_c + K_v \nabla P_v) = - \left( K_l \frac{\partial P_c}{\partial h} + K_v \frac{\partial P_v}{\partial h} \right) \nabla h \quad (1)$$

45 Where  $h$  is the relative humidity,  $P_c$  is the capillary pressure of liquid water,  $P_v$  is the vapor  
 46 pressure. Parameters  $K_l$  and  $K_v$  refer to the permeability of the liquid and vapour, respectively.  
 47  
 48

49 Thus, the mass balance equation can be derived as follows [15, 40, 41]:  
 50

$$\frac{\partial S}{\partial t} = \frac{\partial h}{\partial t} \frac{\partial S}{\partial h} = -\nabla J = \nabla \left( K_l \frac{\partial P_c}{\partial h} + K_v \frac{\partial P_v}{\partial h} \right) \nabla h \quad (2)$$

51  
 52  
 53  
 54  
 55  
 56  
 57  
 58  
 59  
 60  
 61  
 62  
 63  
 64  
 65 where  $S$  is saturation degree. Then, the transport of moisture can be described by introducing  
 66 moisture diffusion coefficient, as [19, 42]:

$$\frac{\partial h}{\partial t} = \nabla (D_l + D_v) \frac{\partial h}{\partial S} \nabla h = \nabla D_h \nabla h \quad (3)$$

82 where  $D_h$ ,  $D_l$  and  $D_v$  refer to moisture, liquid phase and vapour phase diffusion coefficient,  
 1  
 83 respectively ( $\text{m}^2/\text{s}$ ).  $\partial S/\partial h$  is the moisture capacity which represents the slope of water sorption  
 2  
 84 isotherms. For the water wetting process, a relationship between water saturation ( $S_w$ ) and relative  
 3  
 85 humidity can be written as [43, 44]:  
 4  
 86

$$S_w = 1 - \exp \left[ \frac{m_{w/c} - 1}{1.4 \ln \left( \frac{1}{h} \right)} \right] \quad (4)$$

87 where  $m_{w/c}$  is the water to cement ratio. During the drying process, the water isotherm curve is  
 12  
 88 always higher than the corresponding wetting curve because that water can be trapped in larger  
 13  
 89 pores when connected to smaller pores [24]. Thus, the relationship between water saturation ( $S_d$ )  
 14  
 90 and relative humidity during the drying process can be described as [45]:  
 15  
 91

$$S_d = S_w + S_{trap} = S_w(1 - \ln S_w) \quad (5)$$

21  
 92 Considering the moisture capacities for drying and wetting processes are different, the moisture  
 22  
 93 diffusion coefficients should be assigned to the drying and wetting processes respectively as  
 23  
 94 follows [15, 46]:  
 24

$$D_h = \begin{cases} D_d^0 \left[ \alpha + \frac{1 - \alpha}{1 + \left( \frac{1 - h}{1 - h_c} \right)^{n_1}} \right] & \text{drying} \\ D_w^0 \exp(n_2 h) & \text{wetting} \end{cases} \quad (6)$$

30  
 95 where  $D_d^0$  and  $D_w^0$  are the moisture diffusion coefficient of concrete at dry and saturated state,  
 31  
 96 respectively,  $\alpha$  is the ratio of minimum  $D_h$  to  $D_d^0$ ,  $h_c$  is the relative humidity when  $D_h = D_d^0/2$ ,  $n_1$   
 32  
 97 and  $n_2$  refer to the parameters that characterise the spread of drop and rise in moisture diffusion  
 33  
 98 and coefficients. Here,  $\alpha = 0.025$ ,  $h_c = 0.8$ ,  $n_1 = n_2 = 6$  are assumed according to the [46].  
 34  
 99 Considering moisture and heat transfer are coupled together in the present study, Eq. (6) should  
 35  
 100 be modified by taking into account the influenced of temperature, as [23, 47]:  
 36

$$D_h = \begin{cases} D_d^0 \left[ \alpha + \frac{1 - \alpha}{1 + \left( \frac{1 - h}{1 - h_c} \right)^{n_1}} \right] \exp \left[ \frac{U}{R} \left( \frac{1}{T_{ref}} - \frac{1}{T} \right) \right] & \text{drying} \\ D_w^0 \exp(n_2 h) \exp \left[ \frac{U}{R} \left( \frac{1}{T_{ref}} - \frac{1}{T} \right) \right] & \text{wetting} \end{cases} \quad (7)$$

37  
 103 where  $U$  is the activation energy of the diffusion process ( $35000 \text{ J} \cdot \text{mol}$ ),  $R$  is the gas constant  
 38  
 104 ( $8.14 \text{ J} \cdot \text{mol}^{-1} \cdot \text{K}^{-1}$ ),  $T$  is the temperature (K) and  $T_{ref}$  is the reference temperature (296K).  
 39  
 40  
 41  
 42  
 43  
 44  
 45  
 46  
 47  
 48  
 49  
 50  
 51  
 52  
 53  
 54  
 55  
 56  
 57  
 58  
 59  
 60  
 61  
 62  
 63  
 64  
 65

105 The governing equation of heat transfer in unsaturated concrete, excluding convection  
 106 phenomena, can be expressed as [48, 49]:

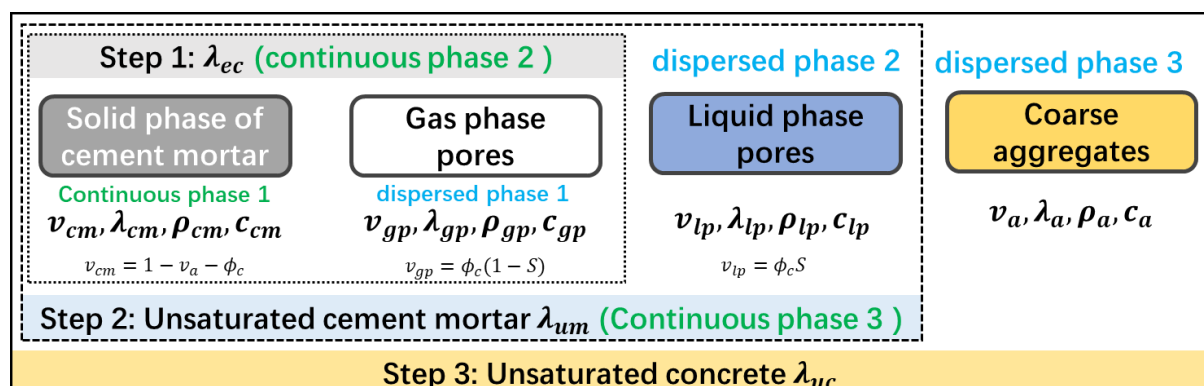
$$107 \quad \rho c(S) \frac{\partial T}{\partial t} = \nabla \frac{\lambda_c(S)}{C_c(S)} \nabla T \quad (8)$$

108 where  $\lambda_c$  and  $C_c$  are thermal conductivity (W/m/K) and thermal capacity (J/m<sup>3</sup>/K) of concrete,  
 109 respectively and  $C_c$  equals to the product of specific heat capacity ( $c$ , J/kg/K) and density  
 110 ( $\rho$ , kg/m<sup>3</sup>) of the material. It is important to note that the heat released and absorbed during the  
 111 condensation and evaporation of moisture is not considered in the present study, as the focus is on  
 112 the overall moisture diffusion process. Considering the effect of moisture transport on heat transfer,  
 113 unsaturated concrete should be regarded as a multi-phase-composite consisting of solid, liquid and  
 114 gaseous phases, which own different thermal conductivities, specific capacities and densities [50].

21 To determine the thermal conductivity of unsaturated concrete, an analytical model will be  
 22 introduced next.

### 26 2.1.2 Thermal conductivity model of unsaturated concrete

28 Due to the heterogeneous nature of concrete, different components of concrete correspond to  
 29 different thermal conductivities [51]. Therefore, this section will take several steps to calculate the  
 30 thermal conductivity of unsaturated concrete, as shown in **Fig. 2**.



49 50 Fig.2 Steps to calculate the thermal conductivity of unsaturated concrete

51 Firstly, at step 1, by treating gas phase pores as the dispersed phase, the effective thermal  
 52 conductivity of cement mortar with gas phases can be obtained by Maxwell's model, which is a  
 53 kind of theoretical model to calculate the effective thermal conductivity of two-phase composite,  
 54 as follows [48, 52]:

$$\lambda_{ec} = \lambda_{cm} \frac{2\lambda_{cm} + \lambda_{gp} - 2(\lambda_{cm} - \lambda_{gp}) \frac{v_{gp}}{v_{gp} + v_{cm}}}{2\lambda_{cm} + \lambda_{gp} + (\lambda_{cm} - \lambda_{gp}) \frac{v_{gp}}{v_{gp} + v_{cm}}} \quad (9)$$

where  $\lambda_{ec}$ ,  $\lambda_{cm}$  and  $\lambda_{gp}$  are the effective thermal conductivity of cement mortar with gas phases, solid phase of cement mortar and gas phase pores, respectively.  $v_{gp}$  and  $v_{cm}$  are volume fraction of gas phase pores and solid phase of cement mortar.

Then, at step 2, unsaturated cement mortar can be considered to be a two-phase composite, which regards liquid phase pores (dispersed phase) are randomly dispersed within cement mortar with gas phase pores (continuous phase, which thermal conductivity has been calculated at step 1). Similarly, the effective thermal conductivity of unsaturated cement mortar can be obtained by Maxwell's model as [53]:

$$\lambda_{um} = \lambda_{ec} \frac{2\lambda_{ec} + \lambda_{lp} - 2(\lambda_{ec} - \lambda_{lp}) \frac{v_{lp}}{v_{gp} + v_{cm} + v_{lp}}}{2\lambda_{ec} + \lambda_{lp} + (\lambda_{ec} - \lambda_{lp}) \frac{v_{lp}}{v_{gp} + v_{cm} + v_{lp}}} \quad (10)$$

where  $\lambda_{um}$  and  $\lambda_{lp}$  are the effective thermal conductivity of unsaturated mortar and liquid phase pores, respectively.  $v_{lp}$  is the volume fraction of liquid phase pores in concrete,  $v_{lp} = S\phi_c$ ;  $\phi_c$  is the porosity of concrete.

Finally, at step 3, assuming that coarse aggregates (dispersed phase) are randomly dispersed in the unsaturated cement mortar (continuous phase). The effective thermal conductivity of unsaturated concrete can also be calculated still by adopting Maxwell's model as:

$$\lambda_{uc} = \lambda_{um} \frac{2\lambda_{um} + \lambda_a - 2(\lambda_{um} - \lambda_a)v_a}{2\lambda_{um} + \lambda_a + (\lambda_{um} - \lambda_a)v_a} \quad (11)$$

where  $\lambda_{uc}$  and  $\lambda_{lp}$  are the effective thermal conductivity of unsaturated concrete and coarse aggregates, respectively. However, it was reported that interfacial resistance would occur between cement mortar and coarse aggregate, and affect the heat transfer. In this case, the effective thermal conductivity of unsaturated concrete should be determined considering interfacial resistance by using Hasselman-Johnson's model [54]:

$$\lambda_{uc} = \lambda_{um} \frac{2\lambda_{um} + \lambda_a(1 + \beta) - 2[\lambda_{um} - \lambda_a(1 - \beta)]v_a}{2\lambda_{um} + \lambda_a(1 + \beta) + [\lambda_{um} - \lambda_a(1 - \beta)]v_a} \quad (12)$$

where  $\beta$  is the interfacial thermal resistance coefficient, depending on the saturation degree of concrete, as [52]:

152 
$$\beta = 0.6369 \cdot S^3 - 1.0338 \cdot S^2 + 0.1728 \cdot S + 0.2235 \quad (13)$$

153 In unsaturated concrete, thermal conductivity can also be calculated based on the volume  
 154 proportions of solid, liquid and gas phases, as [47]:  
 155

156 
$$C_c(S) = (1 - \emptyset_c - v_a)\rho_{cm}c_{cm} + \emptyset_c S \rho_{lp}c_{lp} + \emptyset_c(1 - S)\rho_{gp}c_{gp} + v_a \rho_a c_a \quad (14)$$

157 where  $c_{cm}$   $\rho_{cm}$ ,  $c_{lp}$   $\rho_{lp}$ ,  $c_{gp}$   $\rho_{gp}$  and  $c_a$   $\rho_a$  are the specific heat capacity and density of cement  
 158 mortar, liquid phases, gaseous phases and coarse aggregates, respectively. In the present study, the  
 159 parameters entered to calculate the thermal conductivity of unsaturated concrete are listed in **Table**  
 160

161 **1.** It is important to note that the heat capacities and densities of different phases will also change  
 162 with temperature. However, given that the change is small, it is ignored in the present thermal  
 163 conductivity model [50]. The validation of the proposed thermal conductivity model and the  
 164 coupled moisture and heat transfer model will be carried out in Section 3.1.

165 Table 1 Physical characteristics of solid, liquid and gaseous phases at 293K [48, 50, 52]

Component	$\lambda$ (W/m/K)	$\rho$ (kg/m <sup>3</sup> )	$c$ (J/kg/K)
Cement mortar	1.78	2941.4	920
Gas phase pores	0.0267	1.225	1006.43
Water phase pores	0.58	998.2	4182
Coarse aggregates	2.55	2733	820

## 356 2.2 Chloride transport under varying humidity and temperature changes

### 357 2.2.1 Governing equation

358 Chloride transport in concrete can be regarded as coupling servals basic transport mechanisms,  
 359 such as diffusion, migration, adsorption and pressure-induced flow [31, 55]. In unsaturated  
 360 concrete with no applied electric field, chloride transport mainly depends on chloride diffusion  
 361 caused by the ionic concentration gradient and chloride convection caused by moisture transport  
 362 [6, 56]. The flux of chloride ions  $J_{cl}$  in an unsaturated concrete can be expressed as [57, 58]:

363 
$$J_{cl} = J_{\text{diff}} + J_{\text{conv}} = -D_{cl}(S)\nabla C_{cl} - D_h C_{cl} \nabla h \quad (15)$$

364 where  $J_{\text{diff}}$  and  $J_{\text{conv}}$  are the chloride flux related to chloride diffusion and chloride convection  
 365 (mol/m<sup>2</sup>/s), respectively,  $C_{cl}$  is the total chloride concentration (mol/m<sup>3</sup>),  $D_{cl}(S)$  is the chloride  
 366 diffusion coefficient (m<sup>2</sup>/s), which is strongly related to water saturation. In the present study,  
 367  $D_{cl}(S)$  is assumed as  $D_c \cdot S^r$ , in which  $D_c$  is the chloride diffusion coefficient of saturated concrete  
 368 and  $r = 1$  is parameter [59, 60]. Some empirical or theoretical equations have been developed to  
 369

177 determine the chloride diffusivity of saturated cement paste. This work adopts the equation  
 1  
 178 proposed by Zheng and Zhou [61] which is derived based on the generalized effective medium  
 3  
 179 theory, as:  
 5  
 6

$$180 D_{cp} = \frac{2\phi_{cp}^{2.75} D_0}{\phi_{cp}^{1.75} (1 - \phi_{cp}) + 14.44 (1 - \phi_{cp})^{2.75}} \quad (16)$$

181 where  $D_{cp}$  is the chloride diffusion coefficient of saturated cement paste,  $D_0$  represents the  
 11 chloride diffusion coefficient in pore solution ( $2.03 \times 10^{-9}$ ),  $\phi_{cp}$  is the porosity of the cement  
 12 paste. However, in concrete, the presence of aggregates will increase the effective length travel by  
 13  
 14 a flux. Therefore, by adopting Cidic and Shafikhani formulation for tortuosity factor ( $f_\tau$ ), the  
 15 chloride diffusion coefficient of concrete should be modified as [62]:  
 16  
 17

$$186 D_c = D_{cp} f_\tau = D_{cp} \frac{3(1 - v_a)^2}{3 - v_a} \quad (17)$$

187 Moreover, during chloride transport, some ions react with hydration products to produce  
 25 Friedel's salt, and some are adsorbed on the surface of hydrated calcium silicate or closed between  
 26 the layers of C-S-H, which decelerates the chloride transport. Therefore, the effect of chloride  
 27 binding must be considered during the chloride transport modelling [34, 63]. The relationship  
 28 between total, bound ( $C_b$ ) and free ( $C_f$ ) chloride concentration can be expressed as [33, 64, 65]:  
 29  
 30

$$31 C_{cl} = C_b + S C_f \quad (18)$$

32  
 33 Applying Eq. (15, 18) into mass conversation equation and considering only free chloride can  
 34 transport, the governing equation of chloride transport can be written as:  
 35  
 36

$$37 \frac{\partial C_{cl}}{\partial t} = \left( \frac{\partial C_b}{\partial C_f} + S \right) \frac{\partial C_f}{\partial t} = \nabla (D_c S \nabla C_f + D_h C_f \nabla h) \quad (19)$$

38  
 39 40 By defining  $\frac{\partial C_b}{\partial C_f}$  as  $\gamma$ , it yields:  
 41  
 42

$$43 \frac{\partial C_f}{\partial t} = \nabla \frac{1}{S + \gamma} (D_c S \nabla C_f + D_h C_f \nabla h) \quad (20)$$

44  
 45 46 Under varying humidity and temperature changes, the movement of chloride ions and the  
 47 amount of bound chloride ions can be affected by temperature. Therefore, at different temperatures,  
 48  
 49 50 Eq. (20) should be modified by taking into account the influence of temperature as [49, 66, 67]:  
 51  
 52

$$53 \frac{\partial C_f}{\partial t} = \nabla \frac{1}{S + \gamma(T)} (D_0 S f_T(T) \nabla C_f + D_h C_f f_T(T) \nabla h) \quad (21)$$

$$f_T(T) = \exp \left[ \frac{U}{R} \left( \frac{1}{T_{ref}} - \frac{1}{T} \right) \right] \quad (22)$$

The relationship between bound and free chloride concentration at changed temperatures is still challenging to determine directly. Thus, the present study will propose an empirical binding isotherm by fitting experimental data, as illustrated in the next section.

### 2.2.2 temperature-dependent chloride binding isotherm

For Ordinary Portland Cement (OPC)-based materials, to describe the chloride binding capacity, the linear, Langmuir and Freundlich binding isotherms are often described as follows [12, 68]:

$$C_b = AC_f \quad (23)$$

$$C_b = \frac{AC_f}{1 + BC_f} \quad (24)$$

$$C_b = AC_f^B \quad (25)$$

where  $A$  and  $B$  are binding parameters.

Here, the measured bound chloride concentration under different temperatures and different free chloride concentrations by Dousti and Shekarchi [69], and Panesar et al. [35] are collected, as shown in **Fig. 3**. In Dousti and Shekarchi's work, ASTM Type II OPC was used, with  $m_{w/c}$  of 0.4. NaCl solution of four initial concentrations, 0.1, 0.5, 1 and 3 mol/L were tested. In Panesar et al.'s work, Type I OPC with  $m_{w/c}$  of 0.3 was adopted, and NaCl solution of five initial concentrations, 0.1, 0.5, 0.75, 1, and 3 mol/L were used.

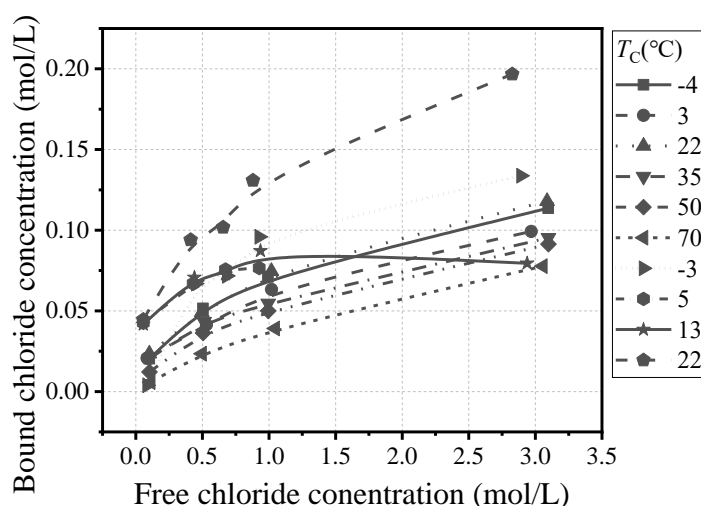


Fig. 3 Measured bound chloride concentration exposed to different temperatures.

222 It can be seen from **Fig. 3** that the linear binding isotherm was too simple to describe the non-  
 1 linear binding capacity accurately. Therefore, Langmuir and Freundlich isotherms are used in this  
 2 section to fit the measured data. **Table 2** summarises the fitted binding parameters ( $A$  and  $B$ ) at  
 3 different temperature. It can be seen that Freundlich isotherm provides a better fitting accuracy. To  
 4 obtain a general relationship that describes the influence of temperature on chloride binding, the  
 5 parameters  $A$  and  $B$  are considered temperature-dependent and expressed as a polynomial function  
 6 of temperature, as follows:  
 7

$$A = a_1 T_C^2 + b_1 T_C + c_1 \quad (26)$$

$$B = a_2 T_C^2 + b_2 T_C + c_2 \quad (27)$$

19 **Fig. 4** shows the parameters  $A$  and  $B$  against exposure temperature for all samples.  $T_C$  denotes  
 20 temperature in degree Celsius. The fitted equations are also shown in the figures. The fitted results  
 21 indicate a non-linear relationship between temperature and the chloride binding capacity. This may  
 22 relate to the fact that while increased temperature can enhance the chemical binding due to an  
 23 increased reaction rate, the physical binding of chloride will be hindered due to the higher thermal  
 24 vibration of chloride ions [69]. In section 3.2, the coupled chloride transport, moisture, and heat  
 25 transfer model will be validated by comparing it with a series of experimental data, including non-  
 26 isothermal chloride transport, chloride transport subjected to drying-wetting cycles and chloride  
 27 transport under varying humidity and temperature changes.  
 28

39 Table 2 Fitted binding parameters by using Langmuir and Freundlich isotherms

T	Langmuir			Freundlich			Ref.
	$A(10^{-1})$	$B(10^{-1})$	$R^2$	$A(10^{-2})$	$B(10^{-1})$	$R^2$	
-4	1.54	10.45	0.9820	6.87	4.57	0.9917	
3	1.23	9.81	0.9416	6.02	4.62	0.9907	
22	1.53	9.76	0.9694	7.02	4.63	0.9966	
35	1.22	9.84	0.9333	5.68	4.54	0.9969	[69]
50	0.897	6.69	0.9855	4.99	5.39	0.9957	
70	0.522	3.47	0.9985	3.67	6.75	0.9958	
-3	2.05	11.69	0.9639	8.56	4.71	0.9099	
5	15.9	200.3	0.9550	7.99	2.14	0.9880	
13	1.44	17.3	0.8810	8.55	2.53	0.9866	[35]
22	3.37	13.9	0.8971	13.1	3.91	0.9897	

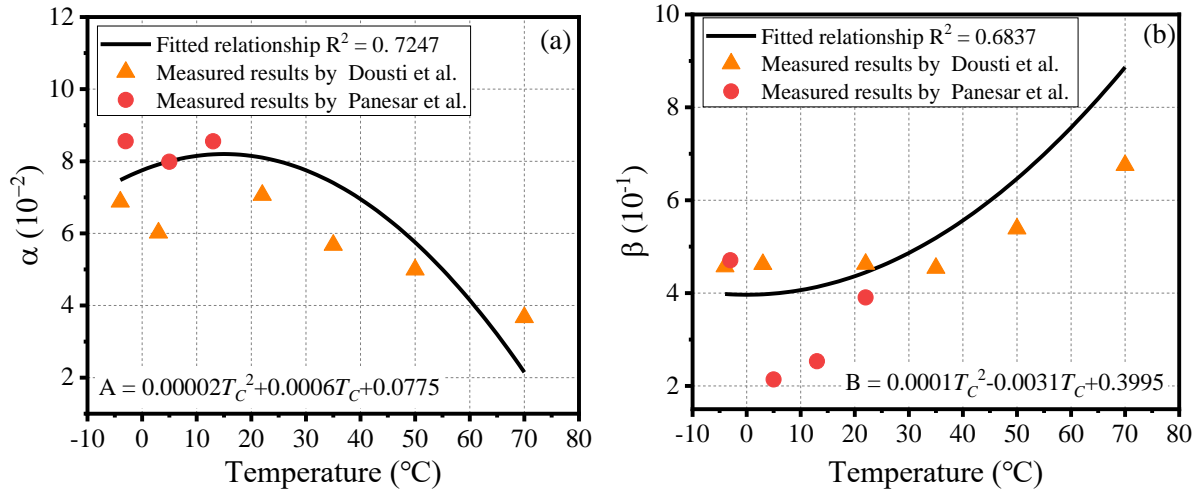


Fig. 4 Relationship between temperature and binding parameters (a) A, (b) B.

### 3. Model validation

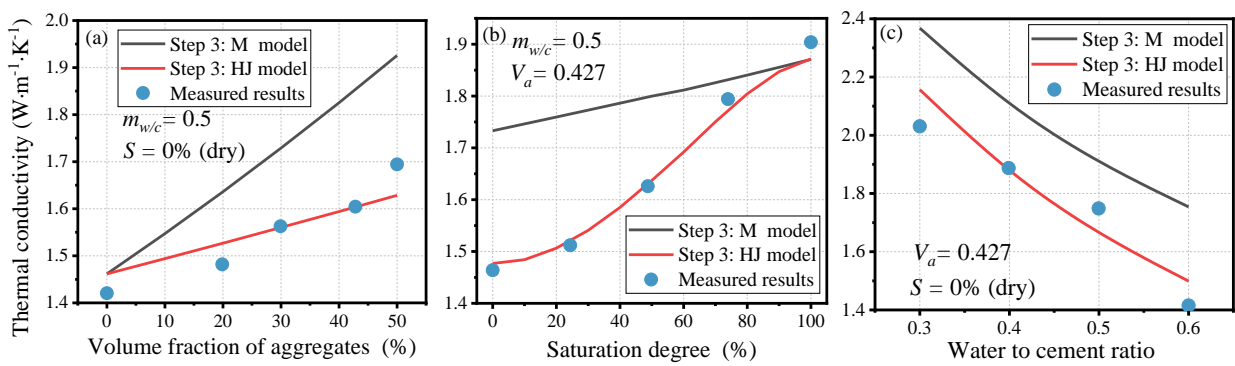
To validate the proposed model of chloride transport in concrete structures under varying humidity and temperature changes, this section will compare the modelled results with a series of published experimental data. Corresponding to the model setup illustrated in section 2, the validation will be done through two sections. Firstly, the thermal conductivity model and coupled moisture and heat transfer model will be validated in section 3.1. Then, the modelling of chloride transport under different environmental conditions will be validated in section 3.2. Since the lateral surfaces of the specimens in the adopted experiments were sealed, the transport processes in concrete can be considered one-dimensional and, therefore, will be modelled in one dimension in this section. Details of experiments will be illustrated in the later sections. The effect of aggregates on chloride transport, moisture and heat transfer process are considered through transport parameters. Parameters used in the proposed model are concluded in Appendix Table A.

#### 3.1 Coupled moisture and heat transfer

##### 3.1.1 Thermal conductivity

To validate the proposed thermal conductivity model, the predicted thermal conductivities of OPC-based concrete with different volume fractions of aggregates, saturation degrees and  $m_{w/c}$  are compared with experimentally measured results from Zhang et al.'s work [52]. In the experiment, OPC with a density of  $3097 \text{ kg/m}^3$  was used. Crushed limestone and natural river sand were used as coarse and fine aggregates, with densities of  $2733 \text{ kg/m}^3$  and  $2639 \text{ kg/m}^3$ , respectively. Thermal conductivities of dry concrete were measured by means of guarded hot plate apparatus [70], while thermal conductivities of unsaturated concrete were measured by means of a transient

264 plane source [71]. Specimens with different volume fractions of aggregates, saturation degree and  
 1  $m_{w/c}$  were all sized at  $250 \times 250 \times 50$  mm. Before measuring thermal conductivity, all  
 2 specimens were kept in a saturated curing room at  $20 \pm 2^\circ\text{C}$  and 95% relative humidity for 28 days.  
 3 Based on the mix proportions, the comparison of modelled and measured results of thermal  
 4 conductivities is shown in Fig. 5.



270 Fig. 5 Comparison of modelled and measured thermal conductivities of concrete with (a) different  
 271 volume fractions of aggregates, (b) saturation degree and (c) water to cement ratio.

272 Notice: M presents using Maxell's model in the 3<sup>rd</sup> step of the model; HJ presents using Hasselman-Johnson's  
 273 model

274 The results indicate Maxell's model would overestimate the thermal conductivities of  
 275 concrete due to the ignorance of interfacial resistance between cement mortar and coarse aggregate.  
 276 On the contrary, the predicted thermal conductivities using Hasselman-Johnson's model in the 3<sup>rd</sup>  
 277 step of the model can obtain reliable results. Because coarse aggregate has a greater conductivity  
 278 than cement mortar, the thermal conductivity of concrete in a dry state will also increase with the  
 279 increasing volume fraction of coarse aggregates, as shown in Fig. 5(a). In the same way, due to  
 280 the thermal conductivity of water being much higher than air, the thermal conductivity of concrete  
 281 increases with the increasing saturation degree, as shown in Fig. 5(b). In addition, considering that  
 282 the porosity (air volume) of concrete increases with the increasing water to cement ratio, thus  
 283 concrete in a dry state has a decreasing thermal conductivity trend with the increasing water to  
 284 cement ratio, as shown in Fig. 5(c).

### 285 3.1.2 Moisture and temperature variation

286 Experimental work done by Wang and Xi [72] is used in this section to validate the coupled  
 287 moisture and heat transfer in concrete. In their experiment, Ordinary type I Portland cement was  
 288 used. The samples were prepared with a water to cement ratio of 0.6 and a gravel to cement ratio

289 of 2.9. After demoulding, cylindrical specimens (6 inch×12inch) were cured at 20 °C and 100%  
 1 relative humidity for 28 days and then kept in the ambient environment to reach the initial  
 2 conditions with 20 °C and 50% relative humidity. In their experiments, the lateral surfaces and  
 3 bottom side were sealed by several layers, including silicone, foam isolation and cable ties to avoid  
 4 exchanges of heat and moisture with the environment. Only the top surface was placed in a  
 5 container filled with distilled water and heated by an electric heater. The boundary and initial  
 6 conditions are given in **Table 3**. The change of temperature and relative humidity inside the sample  
 7 at the position 63.5 mm from the top was measured by the inserted sensors.

1297 Table 3 Boundary and initial conditions of different field variables in concrete [72]

Field variables	Initial conditions		Boundary conditions	
	$h_0$	$T_0$ (K)	$h_s$	$T_s$ (K)
Condition 1	50%	293	100%	313
Condition 2	50%	293	100%	333

298 Notice:  $h_0$  and  $T_0$  are the initial relative humidity and temperature, respectively.  $h_s$  and  $T_s$  are the boundary  
 299 relative humidity and temperature, respectively.

300 **Fig. 6** compares the modelled and measured variation of relative humidity and temperature  
 301 over time at different conditions. The modelled results with and without considering the interaction  
 302 between moisture and heat transfer are also compared. As shown in **Figs. 6 (a-1) and (a-2)**, the  
 303 moisture transport is significantly accelerated by the increased environmental temperature, and the  
 304 influence is obvious at the beginning of the transport process. This is related to the rapid  
 305 temperature growth in the first two days, as shown in **Figs. 6 (b-1) and (b-2)**. After three days, the  
 306 temperature change is relatively small, and the impact on moisture transport is limited. If the  
 307 interaction between moisture and heat transfer is ignored, which means that thermal conductivity  
 308 remains constant at different saturation degrees and moisture diffusion coefficient does not change  
 309 with temperature, the predicted relative humidity and temperature will be underestimated, as  
 310 shown in **Fig. 6**. This is because that the elevated temperature can promote the moisture transport  
 311 and the increased water saturation will also accelerate the heat transfer. The predicted results also  
 312 indicate that considering the interaction relationship for modelling moisture and heat transfer  
 313 processes is important.

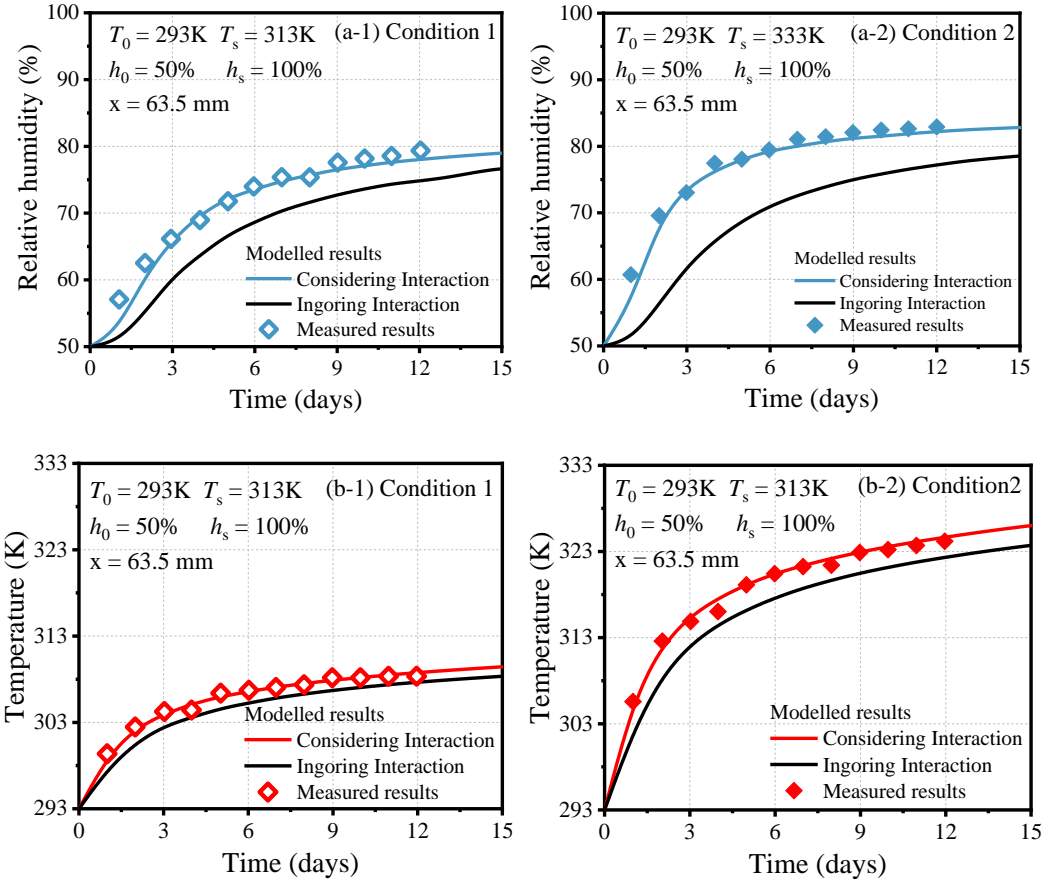


Fig. 6 Comparison of predicted and measured results after exposure to different environmental conditions  
 (a-1) relative humidity variation in condition 1, (a-2) relative humidity variation in condition 2;  
 (b-1) temperature variation in condition 1 (b-2) temperature variation in condition 2.

### 3.2 Chloride transport under different environments

#### 3.2.1 Under the non-isothermal condition

The chloride ingress tests done by Samson and Marchand [49] are used in this section to validate the modelled chloride transport process under non-isothermal conditions. In the experiment, the hydrated cement paste was prepared with an ordinary Canadian Type 10 Portland cement with water to cement ratio of 0.6. The lateral surface of the cylindrical specimens (diameter 10 cm, length 50 mm) was coated with silicon gel. The chloride immersion tests were conducted on saturated cement paste exposed to 0.5 mol/L NaCl solution. The initial temperature of 50-mm specimens was kept at 23 °C, and the immersion test lasted 100 days at 4, 23 and 38 °C, respectively.

**Fig. 7** compares modelled and measured chloride concentration distribution at different immersion temperatures.

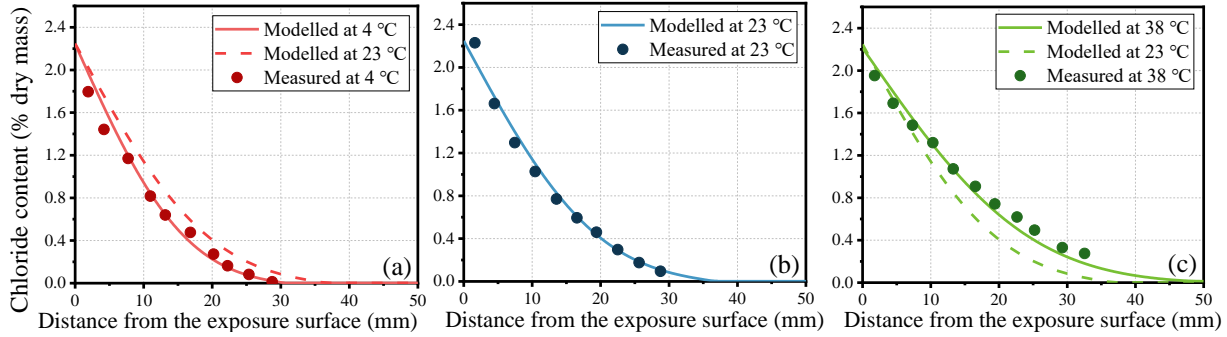


Fig. 7 Comparison of modelled and measured chloride content after 100 days exposure at temperature (a) 4 °C, (b) 23 °C and (c) 38 °C.

The results show a good correlation between the modelled and measured results, and the increased temperature will promote the chloride transport process. The predicted chloride distribution by keeping the constant temperature of 23 °C will overestimate the chloride content at 4 °C and underestimate the chloride content at 38 °C, demonstrating the importance of considering the effect of temperature during chloride transport modelling.

### 3.2.2 Subjected to drying-wetting cycles

This section will validate the modelling of coupled chloride and moisture transport processes while keeping the environmental temperature constant. The chloride transport process in cement mortars exposed to alternate drying-wetting cycles tested by Iqbal and Ishida [60] is chosen to compare with modelled results. In the experiment, all specimens were prepared by OPC with water to cement ratio of 0.5 and sand to cement ratio of 2.25. Specimens consist of cylinders 50 mm in diameter and 100 mm in height. After curing at 20 °C for 28 days, all the specimens were sealed with one face exposed. Then, all the specimens were placed inside an environment control chamber with 60 % relative humidity and 20 °C temperature for 30 days before drying-wetting tests. As shown in Fig. 8, three wetting-to-drying exposure cycles (W/D) were designed weekly to represent the different tidal levels in the marine environment.

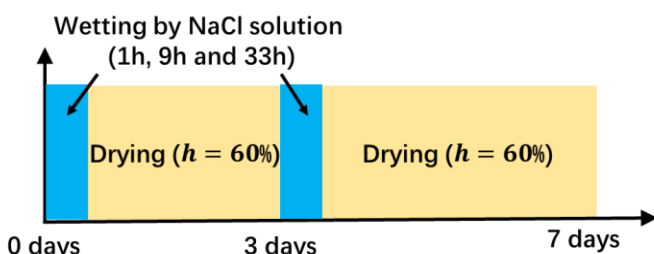


Fig. 8 Weekly exposure cycle for alternate wetting and drying experiment.

After exposing to 6% NaCl solution by mass for 1, 7 and 12 months, the chloride concentration distribution was determined by the slicing method. For the wetting process, Dirichlet boundary conditions with  $C_{cl} = 6\%$  by mass and  $h = 100\%$  are applied to chloride and moisture transport modelling, respectively. On the contrary, the Dirichlet boundary condition with  $h = 60\%$  is applied to moisture transport for the drying process modelling, while the no-flux boundary condition should be used for chloride transport modelling. The comparison of modelled and measured chloride distribution is shown in **Fig. 9**, and good agreements between the two sets of data can be found. It is obvious that the more the number of W/D cycles, the deeper chlorides can penetrate. Due to the cyclic W/D processes, the convection process caused by moisture transport will lead to a significant accumulation of chloride content at the area close to the exposure surface for a long-term period. The chloride distribution profiles obtained by considering combined diffusion and convection processes in **Fig. 9** are obviously different from those shown in Fig. 7, which indicates the importance of considering the effect of moisture transport on chloride penetration under varying relative humidity changes. It can also be found that the increasing wetting time will lead to higher peak values in the chloride contents. However, the penetration depth of chloride ions is generally constant regardless of different W/D conditions.

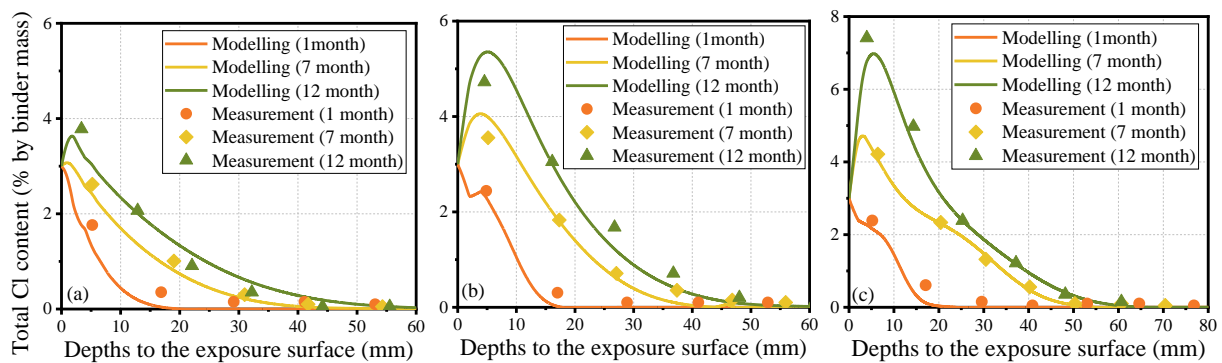


Fig. 9 Comparison of modelled and measured total chloride content during wetting-drying cycles for  
 (a) 1 h wetting, (b) 9 h wetting, (c) 33 h wetting

### 3.2.3 Under cyclic humidity and temperature changes

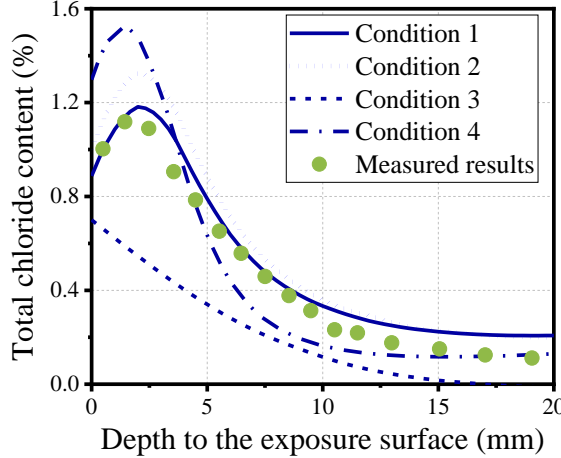
After validating the couple moisture-heat transfer in section 3.1.2, couple heat-chloride transport in section 3.2.1 and coupled moisture-chloride transport in section 3.2.2, respectively, this section will validate the modelling of chloride transport under varying humidity and temperature changes. Herein, the experimental work done by Sun et al. [73] is used. In their research, concretes were prepared with OPC 42.5, water to cement ratio of 0.4, gravel to cement

ratio of 3 and sand to cement ratio of 1.66. The sizes of concrete specimens were set as 100mm × 100mm × 100mm. After being demoulded at 24 h, the specimens were cured at 20 °C and 90 % relative humidity for 27 days. The surface of the specimens for the tests was sealed by epoxy except for one lateral surface. During wetting, specimens will be immersed in 3.5% NaCl solution at 23 °C. Then, the specimens will be dried in an oven at 50 °C. The W/D ratio was set as 1:2.5, and each cycle lasted 3.5 days. The whole experiment lasted 140 days.

The comparison of modelled and measured results is shown in [Fig. 10](#). To further demonstrate the significant influences of environmental variations on chloride penetration, the chloride distributions under assumed environmental conditions (as listed in [Table 4](#)) are also modelled here. It can be seen that the predicted chloride content, considering cyclical relative humidity and temperatures (condition 1), shows a good agreement with measured results. On the contrary, if chloride binding is ignored (condition 2), the chloride content will be overestimated. Besides, when ignoring the effect of moisture transport on chloride penetration (condition 3), the chloride content will be significantly underestimated due to the absence of the convection process. In addition, when temperature remains constant (condition 4), the chloride content will be overestimated in the area near the surface and underestimated in the region away from the surface. This is because the average temperature 42 °C in condition 3 will accelerate the convective process in the wetting process. Overall, from sections 3.1 to 3.2, the series of comparisons on modelled and measured results well demonstrates the effectiveness of the proposed method in terms of modelling the chloride transport under varying humidity and temperature changes.

Table 4 Different environmental conditions used in the model

Environmental conditions	
Condition 1	Relative humidity and temperature change cyclically, with chloride binding
Condition 2	Relative humidity and temperature change cyclically, without chloride binding
Condition 3	Relative humidity remains constant at 100%, and temperature changes cyclically
Condition 4	Relative humidity changes cyclically, temperature remains constant at an average of 42 °C



1  
2  
3  
4  
5  
6  
7  
8  
9  
10  
11  
12  
13  
1498  
1599 Fig. 10 Comparison of modelled and measured total chloride content under cyclic humidity and  
16  
17400 temperature changes

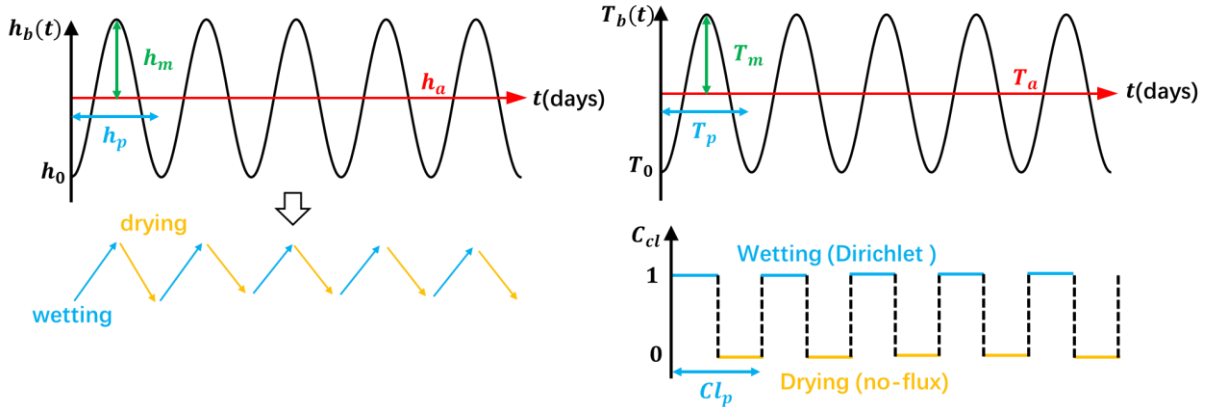
#### 18401 4. Discussion

19402 Under marine or offshore environments, concrete structures are exposed to cyclic wetting-  
20  
21403 drying cycles due to tidal or water splash, and ambient temperature also shows cyclical changes  
22  
23404 throughout the day or over time. Therefore, to better study the cyclic environmental conditions on  
24  
25405 chloride transport, boundary conditions of moisture and heat transfer are assumed as trigonometric  
26  
27406 function (Eqs. (28, 29)), with average  $h_a$  and  $T_a$ , amplitude  $h_m$  and  $T_m$ , as well as period  $h_p$  and  
28  
29407  $T_p$ , accordingly.

$$33408 \quad h_s(t) = h_a + h_m \sin\left(2\pi \frac{t - h_p/4}{h_p}\right) \quad (28)$$

$$35 \quad T_s(t) = T_a + T_m \sin\left(2\pi \frac{t - T_p/4}{T_p}\right) \quad (29)$$

36  
37409 As shown in Fig. 11, the initial humidity and temperature are set as minimum values. During  
40  
41410 repeated wetting and drying cycles, the boundary concentration of chloride transport would  
42  
43411 correspondingly change. Thus, the boundary period of chloride transport is assumed to coincide  
44  
45412 with the boundary period of moisture transport. During wetting, the boundary chloride  
46  
47413 concentration is set as 1 mol/m<sup>3</sup>. The water to cement ratio and volume fraction of coarse  
48  
49414 aggregates of concrete are set as 0.5 and 50%, respectively. In this section, parametric analysis  
50  
51415 will be carried out to study the effect of average value, amplitude value and period length of  
52  
53416 cyclically changed boundary conditions on the chloride transport process.



1  
2  
3  
4  
5  
6  
7  
8  
9  
10  
11  
12 418  
13 419 Fig. 11 Schematic description of the cyclic boundary condition of temperature, relative humidity and  
14  
15 420 chloride concentration.  
16

#### 17 421 4.1 Effect of average value of $h_s(t)$ and $T_s(t)$ on chloride transport 18

19 422 Keeping the amplitude value and period length of boundary conditions constant, the section  
20  
21 423 compares chloride concentration profiles after 200 days of exposure at different average boundary  
22  
23 424 humidity and temperature values. The detailed input parameters of  $h_s(t)$  and  $T_s(t)$  are listed in  
24  
25 425 **Table 5**.  
26

27 426 Table 5 Input parameters of boundary humidity and temperature with changes in average values  
28

Condition	$h_a$	$h_m$	$h_p$	$T_a$	$T_m$	$T_p$	Results
$h_a$ changes	50%						
	60%						
	70%	20%	10 (days)	298 K	10 K	10 (days)	Fig. 12(a)
	80%						
$T_a$ changes				288 K			
				293 K			
				298 K			
				303 K			
					10 K	10 (days)	Fig. 12(b)

45 427 Fig. 12 shows the modelled total chloride concentration after 200 days. It can be found that  
46  
47 increased average humidity or temperature would lead to higher chloride concentration and peak  
48 values. Besides, as shown in Fig. 12(a), increased average humidity will not only promote the  
49 peak values but also the peak location of chloride distribution and penetration depths of chloride  
50  
51 penetration slightly. This is because the higher average environmental humidity gives the concrete  
52 a higher saturation degree, which can accelerate the moisture and chloride transport. On the  
53  
54 contrary, as shown in Fig. 12(b), increased average temperature mainly affects the peak values of  
55 total chloride concentrations, while the peak locations and penetration depths remain generally  
56  
57  
58 433 total chloride concentrations, while the peak locations and penetration depths remain generally  
59  
60  
61 434

constant. This also indicates that the chloride penetration depth is mainly dominated by moisture transport during the cyclic wetting-drying processes.

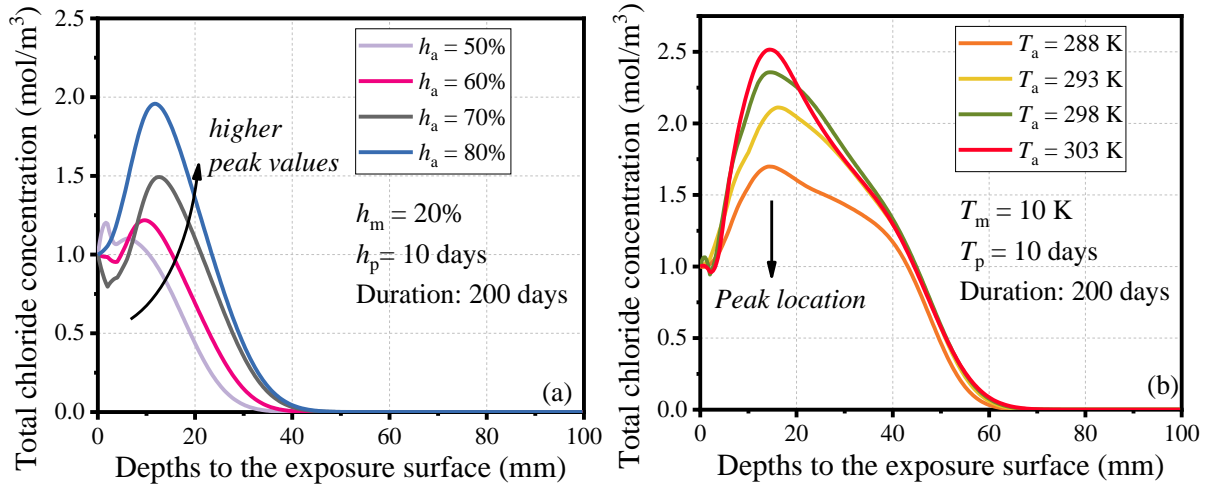


Fig. 12 Chloride concentration profiles at different average values of (a)  $h_s(t)$  and (b)  $T_s(t)$

#### 4.2 Effect of amplitude value of $h_s(t)$ and $T_s(t)$ on chloride transport

Similar to section 4.1, this section remains the average value and period length of boundary conditions constant and compares chloride concentration profiles after 200 days of exposure at different amplitude values of boundary humidity and temperature. The detailed input parameters of  $h_s(t)$  and  $T_s(t)$  are listed in **Table 6**.

Table 6 Input parameters of boundary humidity and temperature with changed amplitude values

Condition	$h_a$	$h_m$	$h_p$	$T_a$	$T_m$	$T_p$	Results
$h_m$ changes	60%	10%					
		20%					
		30%	10 (days)	298 K	10 K	10 (days)	Fig. 13(a)
		40%					
$T_m$ changes	60%				5 K 10 K 15 K 20 K		
		40%	10 (days)	298 K		10 (days)	Fig. 13(b)

The predicted total chloride concentration profiles are shown in **Fig. 13**. It is apparent from

**Fig. 13(a)** that as the humidity amplitude increases, there is a substantial increase in peak values, peak locations and the penetration depths of chloride ions. This is because an increase in boundary humidity amplitudes over the same period can lead to more intense chloride convection processes. This finding also agrees with Chen et al.'s experiments [74]. However, as shown in **Fig. 13(b)**,

chloride distributions have less variability when the average temperature is held constant and the boundary temperature amplitudes gradually increase. This is because while an increase in temperature amplitude raises the temperature during half of the time and can accelerate the transport process, the temperature will also decrease in the other half and hinder the transport process. So, the two effects cancel each other, making the final concentration distribution less variable.

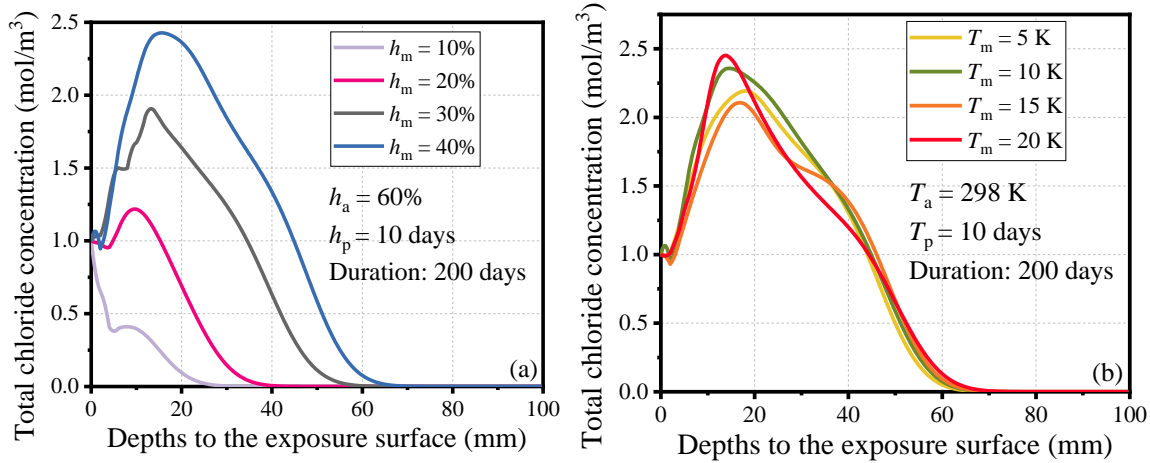


Fig. 13 Chloride concentration profiles at different amplitude values of (a)  $h_s(t)$  and (b)  $T_s(t)$

### 4.3 Effect of period length of $h_s(t)$ and $T_s(t)$ on chloride transport

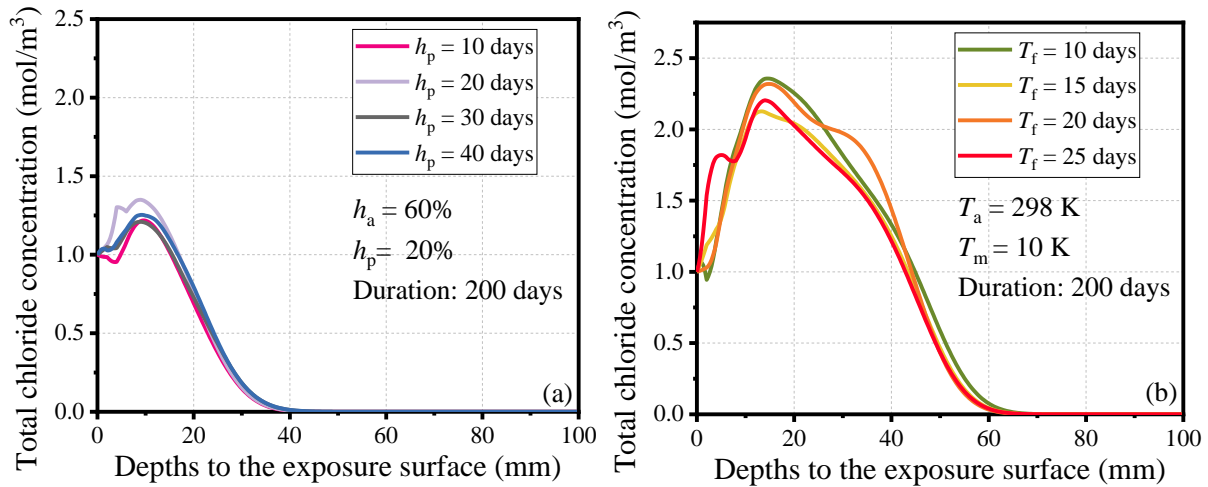
Finally, this section remains the average and amplitude value of boundary conditions constant and compares chloride concentration profiles under different period lengths of boundary humidity and temperature. The detailed input parameters of  $h_s(t)$  and  $T_s(t)$  are listed in **Table 7**.

Table 7 Input parameters of boundary humidity and temperature with changed amplitude values

Condition	$h_a$	$h_m$	$h_p$	$T_a$	$T_m$	$T_p$	Results
$h_p$ changes	60%	20%	10 (days)	298 K	10 K	10 (days)	Fig. 14(a)
			20 (days)				
			30 (days)				
			40 (days)				
$T_p$ changes	60%	40%	10 (days)	298 K	10 K	10 (days)	Fig. 14(b)
						15 (days)	
						20 (days)	
						25 (days)	

Fig. 14 shows the modelled total chloride concentration after 200 days. When the exposure time is the same, a longer period also implies a decrease in the number of cycles. So, it can be seen

465 from the figures that the increase in period length has less effect on the final chloride distribution  
 1 profiles. Combining sections 4.1, 4.2 and 4.3, it can be concluded that the variation of humidity  
 2 and temperature average can alter the peak values of chloride content but has less effect on the  
 3 chloride penetration depth. However, the humidity amplitude change during cyclic wetting-drying  
 4 processes could significantly affect both the peaks and the penetration depths, whereas other  
 5 factors have less impact on the chloride transport process at a constant exposure time.  
 6  
 7  
 8  
 9  
 10  
 11



30 Fig. 14 Chloride concentration profiles at different period lengths of (a)  $h_s(t)$  and (b)  $T_s(t)$

## 31 5. Conclusions

32 This study proposed a numerical model to investigate the chloride penetration in concrete  
 33 under varying humidity and temperature changes. The interaction between moisture and heat  
 34 transfer and their coupled effect on chloride transport are analysed. The predicted chloride  
 35 distributions under different environments are compared with published experimental data. The  
 36 following conclusions can be drawn:  
 37  
 38

39 (1) Considering the heterogeneous features of unsaturated concrete, the thermal conductivities of  
 40 concretes with different volume fractions of aggregates, saturation degree and  $m_{w/c}$  can be  
 41 predicted through the proposed thermal conductivity model. The predicted results show that  
 42 the thermal conductivity of concrete in a dry state will also increase with the increasing volume  
 43 fraction of coarse aggregates and saturation degree. In contrast, it has a decreasing trend with  
 44 the rising water to cement ratio.  
 45  
 46 (2) For the coupled moisture and heat transfer, the elevated temperature can promote moisture  
 47 transport, and the increased water saturation will also accelerate the heat transfer. If the  
 48

487 interaction between moisture and heat transfer is ignored, the predicted relative humidity and  
1  
488 temperature will be underestimated.  
3

489 (3) The chloride transport under varying humidity and temperature changes depends on the  
5 combined chloride diffusion and convection processes. The increased temperature will  
7 promote the chloride transport process. A non-linear relationship exists between temperature  
8 and the chloride binding capacity. Due to the cyclic W/D processes, the convection process  
9 will significantly accumulate chloride content near the exposure surface. The increasing  
10 wetting time will lead to higher peak values in the chloride contents. However, the penetration  
11 depth of chloride ions is generally constant regardless of different W/D conditions.  
12  
13  
14  
15  
16  
17  
18

196 (4) The proposed model can analyse the effect of average value, amplitude value and period length  
20 of cyclic environmental changes on the chloride transport process by assuming boundary  
21 conditions of moisture and heat transfer as trigonometric functions. The results indicate that  
22 variation in humidity and temperature averages can alter the peak values of chloride content  
23 but have less effect on the chloride penetration depth. However, the increased humidity  
24 amplitude could significantly promote both the peak values and the penetration depths,  
25 whereas other factors have less impact on the chloride transport process at a constant exposure  
26 time.  
27  
28  
29  
30  
31  
32  
33  
34  
35

36 The present study introduces a one-dimensional numerical model for chloride penetration in  
37 OPC concrete under varying humidity and temperature conditions. However, several areas require  
38 further investigation. First, the model should be expanded from one-dimensional to two-  
39 dimensional or even three-dimensional to better represent real-world scenarios. Additionally,  
40 future work should further incorporate the coupling of moisture and heat transfer by considering  
41 the heat released and absorbed during the condensation and evaporation of moisture.  
42  
43  
44  
45  
46  
47  
48  
49  
50  
51  
52

## 53 Acknowledgements

54 This work was funded by the National Natural Science Foundation of China (52222805), the  
55 Natural Science Foundation of Shanghai, China (22ZR1431400), and the Open Foundation of the  
56 State Key Laboratory of Subtropical Building and Urban Science (2023KA03).  
57  
58

## 59 Appendix

Table A Parameters used in the proposed model

Parameters	Values or expressions	References
<b>Coupled moisture and heat transfer</b>		
$D_d^{\text{ref}}$	Moisture reference diffusion coefficient during drying process	$8.31 \times 10^{-10} \text{ m}^2/\text{s}$ [15]
$D_w^{\text{ref}}$	Moisture reference diffusion coefficient during wetting process	$4.05 \times 10^{-11} \text{ m}^2/\text{s}$ [15]
$D_d^0$	Moisture diffusion coefficient of concrete at dry state	$D_d^{\text{ref}} \frac{3(1 - v_a)^2}{3 - v_a}$ [62]
$D_w^0$	Moisture diffusion coefficient of concrete at saturated state	$D_w^{\text{ref}} \frac{3(1 - v_a)^2}{3 - v_a}$ [62]
$h_c$	Relative humidity when $D_h = D_d^0/2$	0.8
$\alpha$	Ratio of minimum $D_h$ to $D_d^0$	0.025 [46]
$n_1$	Regression coefficient	6
$n_2$	Regression coefficient	6
$U$	Activation energy of the diffusion process	35000J/mol [15]
$R$	Gas constant	$8.14 \text{ J} \cdot \text{mol}^{-1} \cdot \text{K}^{-1}$ [31]
$T_{\text{ref}}$	Reference temperature	296K [75]
$\rho$	Density	Table 1 (including gas pores, liquid pores, aggregates and cement mortar)
$c$	Specific heat capacity	Table 1 (including gas pores, liquid pores, aggregates and cement mortar) [48, 50, 52]
$\lambda$	Thermal conductivity	
$v_a$	Volume fraction of aggregates	Experimental mixtures
$m_{w/c}$	Water to cement ratio	Experimental mixtures
$\alpha_{\text{HD}}$	Hydration degree of cement paste	$1 - \exp(-3.15m_{w/c})$ [33]
$\phi_{\text{cp}}$	Porosity of cement paste	$\frac{m_{w/c} - 0.36\alpha_{\text{HD}}}{m_{w/c} + 0.32}$ [51]
$\phi_c$	Porosity of concrete	$\phi_{\text{cp}}(1 - v_a)$ [48]
<b>Chloride transport under varying humidity and temperature changes</b>		
$D_0$	Chloride diffusivity in pore solution	$2.03 \times 10^{-9}$ [76]
$D_{\text{cp}}$	Chloride diffusivity of saturated cement paste	$\frac{2\phi_{\text{cp}}^{2.75}D_0}{\phi_{\text{cp}}^{1.75}(1 - \phi_{\text{cp}}) + 14.44(1 - \phi_{\text{cp}})^{2.75}}$ [61]
$D_c$	Chloride diffusivity of saturated concrete considering the presence of aggregates	$D_{\text{cp}} \frac{3(1 - v_a)^2}{3 - v_a}$ [62]
$r$	Impact index of water saturation	1 [15]
$A$	Chloride binding parameters fitted based on experimental data	$0.00002T_c^2 + 0.0006T_c + 0.0775$ [35, 69]
$B$		$0.0001T_c^2 - 0.0031T_c + 0.3995$

## References

[1] Wang H-L, Dai J-G, Sun X-Y, and Zhang X-L, *Characteristics of concrete cracks and their influence on chloride penetration*. Construction and Building Materials, 2016, **107**: 216-225.

[2] Meng Z, Liu Q-f, Xia J, Cai Y, Zhu X, Zhou Y, and Pel L, *Mechanical-transport-chemical modeling of electrochemical repair methods for corrosion-induced cracking in marine concrete*. Computer-Aided Civil and Infrastructure Engineering, 2022, **37**(14): 1854-1874.

[3] Tongning C, Lijuan Z, Guowen S, Caihui W, Ying Z, Pengshuo W, and Aoxue X, *Simulation of chloride ion transport in concrete under the coupled effects of a bending load and drying-wetting cycles*. Construction and Building Materials, 2020, **241**: 118045.

526 [4] Yu Z, Chen Y, Liu P, and Wang W, *Accelerated simulation of chloride ingress into concrete under*  
527 *drying-wetting alternation condition chloride environment*. Construction and Building Materials,  
528 2015, **93**: 205-213.

529 [5] Liu Q-f, *Progress and research challenges in concrete durability: ionic transport, electrochemical*  
530 *rehabilitation and service life prediction*. RILEM Technical Letters, 2022, **7**: 98-111.

531 [6] Homan L, Ababneh A N, and Xi Y, *The effect of moisture transport on chloride penetration in concrete*.  
532 Construction and Building Materials, 2016, **125**: 1189-1195.

533 [7] Nielsen E P and Geiker M R, *Chloride diffusion in partially saturated cementitious material*. Cement  
534 and Concrete Research, 2003, **33**(1): 133-138.

535 [8] Ishida T, Maekawa K, and Kishi T, *Enhanced modeling of moisture equilibrium and transport in*  
536 *cementitious materials under arbitrary temperature and relative humidity history*. Cement and  
537 concrete research, 2007, **37**(4): 565-578.

538 [9] Zheng H, Dai J-G, Li W, and Poon C S, *Influence of chloride ion on depassivation of passive film on*  
539 *galvanized steel bars in concrete pore solution*. Construction and Building Materials, 2018, **166**:  
540 572-580.

541 [10] Xiong Q X, Tong L-y, Zhang Z, Shi C, and Liu Q-f, *A new analytical method to predict permeability*  
542 *properties of cementitious mortars: the impacts of pore structure evolutions and relative humidity*  
543 *variations*. . Cement and Concrete Composites, 2023, **137**: 104912.

544 [11] Sun G, Zhang Y, Sun W, Liu Z, and Wang C, *Multi-scale prediction of the effective chloride diffusion*  
545 *coefficient of concrete*. Construction and Building Materials, 2011, **25**(10): 3820-3831.

546 [12] Tong L, Zhao J, and Cheng Z, *Chloride ion binding effect and corrosion resistance of geopolymers*  
547 *materials prepared with seawater and coral sand*. Construction and Building Materials, 2021, **309**:  
548 125126.

549 [13] Olsson N, Baroghel-Bouny V, Nilsson L-O, and Thiery M, *Non-saturated ion diffusion in concrete –*  
550 *A new approach to evaluate conductivity measurements*. Cement and Concrete Composites, 2013,  
551 **40**: 40-47.

552 [14] Yang L F, Cai R, and Yu B, *Investigation of computational model for surface chloride concentration*  
553 *of concrete in marine atmosphere zone*. Ocean Engineering, 2017, **138**: 105-111.

554 [15] Chen D, Yang K, Hu D, and Shi J, *A meso-stochastic research on the chloride transport in unsaturated*  
555 *concrete*. Construction and Building Materials, 2021, **273**: 121986.

556 [16] Zhang Y, Yang Z, and Ye G, *Dependence of unsaturated chloride diffusion on the pore structure in*  
557 *cementitious materials*. Cement and Concrete Research, 2020, **127**: 105919.

558 [17] Zhang Y and Zhang M, *Transport properties in unsaturated cement-based materials–A review*.  
559 Construction and Building Materials, 2014, **72**: 367-379.

560 [18] Zhu J-H, Zeng C, Su M-n, Zeng Z-w, and Zhu A, *Effectiveness of a dual-functional intervention method*  
561 *on the durability of reinforced concrete beams in marine environment*. Construction and Building  
562 Materials, 2019, **222**: 633-642.

563 [19] Li K, Li C, and Chen Z, *Influential depth of moisture transport in concrete subject to drying-wetting*  
564 *cycles*. Cement and Concrete Composites, 2009, **31**(10): 693-698.

565 [20] Zhang Z, Thiery M, and Baroghel-Bouny V, *Numerical modelling of moisture transfers with hysteresis*  
566 *within cementitious materials: Verification and investigation of the effects of repeated wetting–*  
567 *drying boundary conditions*. Cement and Concrete Research, 2015, **68**: 10-23.

568 [21] Li W and Guo L, *Peridynamic investigation of chloride diffusion in concrete under typical*  
 569 *environmental factors*. Ocean Engineering, 2021, **239**: 109770.

570 [22] Lian S, Meng T, Zhao Y, Liu Z, Zhou X, and Ruan S, *Experimental and theoretical analyses of chloride*  
 571 *transport in recycled concrete subjected to a cyclic drying-wetting environment*. Structures, 2023,  
 572 **52**: 1020-1034.

573 [23] Bai Y, Wang Y, and Xi Y, *Modeling the effect of temperature gradient on moisture and ionic transport*  
 574 *in concrete*. Cement and Concrete Composites, 2020, **106**: 103454.

575 [24] Jiang Z, Xi Y, Gu X, Huang Q, and Zhang W, *Modelling of water vapour sorption hysteresis of cement-*  
 576 *based materials based on pore size distribution*. Cement and Concrete Research, 2019, **115**: 8-19.

577 [25] Isteita M and Xi Y, *The effect of temperature variation on chloride penetration in concrete*.  
 578 Construction and Building Materials, 2017, **156**: 73-82.

579 [26] Zhao H, Jiang K, Yang R, Tang Y, and Liu J, *Experimental and theoretical analysis on coupled effect*  
 580 *of hydration, temperature and humidity in early-age cement-based materials*. International Journal  
 581 of Heat and Mass Transfer, 2020, **146**: 118784.

582 [27] Care S, *Effect of temperature on porosity and on chloride diffusion in cement pastes*. Construction and  
 583 Building Materials, 2008, **22**(7): 1560-1573.

584 [28] Nguyen T, Lorente S, and Carcasses M, *Effect of the environment temperature on the chloride diffusion*  
 585 *through CEM-I and CEM-V mortars: An experimental study*. Construction and Building Materials,  
 586 2009, **23**(2): 795-803.

587 [29] Tong L-y and Liu Q-f, *Modelling of concrete transport property by considering multi-scale*  
 588 *heterogeneous characteristics*. Journal of Building Materials, 2023, **26**(10): 1062-1071.

589 [30] Tong L-y and Liu Q-f, *Prediction Model for Diffusivity of Unsaturated Concrete by Considering Time-*  
 590 *Varying Pore Structure*. Journal of the Chinese Ceramic Society, 2023, **51**(8): 1950-1961.

591 [31] Liu Q-f, Feng G-l, Xia J, Yang J, and Li L-y, *Ionic transport features in concrete composites containing*  
 592 *various shaped aggregates: a numerical study*. Composite Structures, 2018, **183**: 371-380.

593 [32] Yang S, Ukrainczyk N, Caggiano A, and Koenders E, *Numerical phase-field model validation for*  
 594 *dissolution of minerals*. Applied Sciences (Switzerland), 2021, **11**(6).

595 [33] Jiang W-q, Shen X-h, Hong S, Wu Z-y, and Liu Q-f, *Binding capacity and diffusivity of concrete*  
 596 *subjected to freeze-thaw and chloride attack: A numerical study*. Ocean Engineering, 2019, **186**:  
 597 106093.

598 [34] Fenaux M, Reyes E, Gálvez J C, and Moragues A, *Modelling the transport of chloride and other ions*  
 599 *in cement-based materials*. Cement and Concrete Composites, 2019, **97**: 33-42.

600 [35] Panesar D K and Chidiac S E, *Effect of Cold Temperature on the Chloride-Binding Capacity of Cement*.  
 601 Journal of Cold Regions Engineering, 2011, **25**(4): 133-144.

602 [36] Ecay L, Grégoire D, and Pijaudier-Cabot G, *On the prediction of permeability and relative permeability*  
 603 *from pore size distributions*. Cement and Concrete Research, 2020, **133**: 106074.

604 [37] Gimmi T and Churakov S V, *Water retention and diffusion in unsaturated clays: Connecting atomistic*  
 605 *and pore scale simulations*. Applied Clay Science, 2019, **175**: 169-183.

606 [38] Li L-y, *A pore size distribution-based chloride transport model in concrete*. Magazine of Concrete  
 607 Research, 2014, **66**(18): 937-947.

608 [39] Ren F, Chen X, Zeng Q, and Zhou C, *Effects of pure carbonation on pore structure and water*  
 609 *permeability of white cement mortars*. Cement, 2022, **9**: 100040.

610 [40] Kang S-T, Kim J-S, Lee Y, Park Y-D, and Kim J-K, *Moisture diffusivity of early age concrete*  
611 *considering temperature and porosity*. KSCE Journal of Civil Engineering, 2011, **16**(1): 179-188.

612 [41] Tong L-y, Xiong Q X, Zhang Z, Chen X, Ye G, and Liu Q-f, *A novel lattice model to predict chloride*  
613 *diffusion coefficient of unsaturated cementitious materials based on multi-typed pore structure*  
614 *characteristics*. Cement and Concrete Research, 2024, **176**: 107351.

615 [42] Cho B, Park D, Kim J, and Hamasaki H, *Study on the heat-moisture transfer in concrete under real*  
616 *environment*. Construction and Building Materials, 2017, **132**: 124-129.

617 [43] Bahador S D and Cahyadi J H, *Modelling of carbonation of PC and blended cement concrete*. The IES  
618 *Journal Part A: Civil & Structural Engineering*, 2009, **2**(1): 59-67.

619 [44] Liu P, Yu Z, and Chen Y, *Carbonation depth model and carbonated acceleration rate of concrete under*  
620 *different environment*. Cement and Concrete Composites, 2020, **114**: 103736.

621 [45] Li J, Xie F, Zhao G, and Li L, *Experimental and numerical investigation of cast-in-situ concrete under*  
622 *external sulfate attack and drying-wetting cycles*. Construction and Building Materials, 2020, **249**.

623 [46] Saetta A V, Schrefler B A, and Vitaliani R V, *The carbonation of concrete and the mechanism of*  
624 *moisture, heat and carbon dioxide flow through porous materials*. Cement and Concrete Research, 1993,  
625 **23**(4): 761-772.

626 [47] Chen X, Sanchez T, Conciatori D, Chaouki H, Sorelli L, Selma B, and Chekired M, *Numerical*  
627 *modeling of 2D hygro-thermal transport in unsaturated concrete with capillary suction*. Journal of  
628 *Building Engineering*, 2022, **45**.

629 [48] Zhang S, Zhou H, and Wang H, *Thermal conductive properties of solid-liquid-gas three-phase*  
630 *unsaturated concrete*. Construction and Building Materials, 2020, **232**: 117242.

631 [49] Samson E and Marchand J, *Modeling the effect of temperature on ionic transport in cementitious*  
632 *materials*. Cement and Concrete Research, 2007, **37**(3): 455-468.

633 [50] Kim K-H, Jeon S-E, Kim J-K, and Yang S, *An experimental study on thermal conductivity of concrete*.  
634 *Cement and Concrete Research*, 2003, **33**(3): 363-371.

635 [51] Tong L-y, Xiong Q X, Zhang M, Meng Z, Meftah F, and Liu Q-f, *Multi-scale modelling and statistical*  
636 *analysis of heterogeneous characteristics effect on chloride transport properties in concrete*.  
637 *Construction and Building Materials*, 2023, **367**: 130096.

638 [52] Zhang W, Min H, Gu X, Xi Y, and Xing Y, *Mesoscale model for thermal conductivity of concrete*.  
639 *Construction and Building Materials*, 2015, **98**: 8-16.

640 [53] Boomsma K and Poulikakos D, *On the effective thermal conductivity of a three-dimensionally*  
641 *structured fluid-saturated metal foam*. International Journal of Heat and Mass Transfer, 2001,  
642 **44**(4): 827-836.

643 [54] Hasselman D P H and Johnson L F, *Effective Thermal Conductivity of Composites with Interfacial*  
644 *Thermal Barrier Resistance*. Journal of Composite Materials, 1987, **21**(6): 508-515.

645 [55] Liu Q-f, Easterbrook D, Yang J, and Li L-y, *A three-phase, multi-component ionic transport model for*  
646 *simulation of chloride penetration in concrete*. Engineering Structures, 2015, **86**: 122-133.

647 [56] Nguyen T Q, Petković J, Dangla P, and Baroghel-Bouny V, *Modelling of coupled ion and moisture*  
648 *transport in porous building materials*. Construction and Building Materials, 2008, **22**(11): 2185-  
649 2195.

650 [57] Chen W-k and Liu Q-f, *Moisture and multi-ions transport in concrete under drying-wetting cycles: a*  
651 *numerical study*. SHUILI XUEBAO, 2021, **52**(5): 622-632.

652 [58] Meng Z, Zhang Y, Chen W-k, Fu C-q, Xiong Q X, Zhang C-l, and Liu Q-f, *A Numerical Study of*  
653 *Moisture and Ionic Transport in Unsaturated Concrete by Considering Multi-ions Coupling Effect.*  
654 *Transport in Porous Media*, 2024, **151**(2): 339-366.

655 [59] Nizovtsev M, Stankus S, Sterlyagov A, Terekhov V, and Khairulin R, *Determination of moisture*  
656 *diffusivity in porous materials using gamma-method*. *International Journal of Heat and Mass*  
657 *Transfer*, 2008, **51**(17-18): 4161-4167.

658 [60] O'Neill Iqbal P and Ishida T, *Modeling of chloride transport coupled with enhanced moisture*  
659 *conductivity in concrete exposed to marine environment*. *Cement and Concrete Research*, 2009,  
660 **39**(4): 329-339.

661 [61] Zheng J and Xinzhu Z, *Analytical solution for the chloride diffusivity of hardened cement paste*. *Journal*  
662 *of Materials in Civil Engineering*, 2008, **20**(5): 384-391.

663 [62] Chidiac S E and Shafikhani M, *Phenomenological model for quantifying concrete chloride diffusion*  
664 *coefficient*. *Construction and Building Materials*, 2019, **224**: 773-784.

665 [63] Xu J, Song Y, Jiang L, Feng W, Cao Y, and Ji W, *Influence of elevated temperature on release of bound*  
666 *chlorides from chloride-admixed plain and blended cement pastes*. *Construction and Building*  
667 *Materials*, 2016, **104**: 9-15.

668 [64] Jiang W-q, Shen X-h, Xia J, Mao L-x, Yang J, and Liu Q-f, *A numerical study on chloride diffusion in*  
669 *freeze-thaw affected concrete*. *Construction and Building Materials*, 2018, **179**: 553-565.

670 [65] Liu Q-f, Cai Y, Peng H, Meng Z, Mundra S, and Castel A, *A numerical study on chloride transport in*  
671 *alkali-activated fly ash/slag concretes*. *Cement and Concrete Research*, 2023, **166**: 107094.

672 [66] Damrongwiriyapan N, Li L, Limkatanyu S, and Xi Y, *Temperature effect on multi-ionic species*  
673 *diffusion in saturated concrete*. *Computers and Concrete*, 2014, **13**(2): 149-171.

674 [67] Yu Y, Chen X, Gao W, Wu D, and Castel A, *Modelling non-isothermal chloride ingress in unsaturated*  
675 *cement-based materials*. *Construction and Building Materials*, 2019, **217**: 441-455.

676 [68] Li J and Shao W, *The effect of chloride binding on the predicted service life of RC pipe piles exposed*  
677 *to marine environments*. *Ocean Engineering*, 2014, **88**: 55-62.

678 [69] Dousti A and Shekarchi M, *Effect of exposure temperature on chloride-binding capacity of cementing*  
679 *materials*. *Magazine of Concrete Research*, 2015, **67**(15): 821-832.

680 [70] ISO, *Thermal insulation-Determination of steady-state thermal resistance and related properties-Heat*  
681 *flow meter apparatus*. ISO (International Organization for Standardization), Geneva, Switzerland,  
682 1991.

683 [71] Gustafsson S E, *Transient plane source techniques for thermal conductivity and thermal diffusivity*  
684 *measurements of solid materials*. *Review of Scientific Instruments*, 1991, **62**(3): 797-804.

685 [72] Wang Y and Xi Y, *The Effect of Temperature on Moisture Transport in Concrete*. *Materials* (Basel),  
686 2017, **10**(8).

687 [73] Sun C, Yuan L, Zhai X, Qu F, Li Y, and Hou B, *Numerical and experimental study of moisture and*  
688 *chloride transport in unsaturated concrete*. *Construction and Building Materials*, 2018, **189**: 1067-  
689 1075.

690 [74] Chen C, Wang L, Liu R, Zhu P, Liu H, Wang X, Yu J, and Chen Y, *Chloride penetration of concrete*  
691 *exposed to dry-wet cycle with various dry-wet ratios and temperature*. *Construction and Building*  
692 *Materials*, 2023, **400**.

693 [75] Zhu X, Zi G, Cao Z, and Cheng X, *Combined effect of carbonation and chloride ingress in concrete*.  
694 *Construction and Building Materials*, 2016, **110**: 369-380.

695 [76] Achour M, Bignonnet F, Barthélémy J-F, Rozière E, and Amiri O, *Multi-scale modeling of the chloride  
696 diffusivity and the elasticity of Portland cement paste*. Construction and Building Materials, 2020,  
697 234: 117124.  
698

5

6

7

8

9

10

11

12

13

14

15

16

17

18

19

20

21

22

23

24

25

26

27

28

29

30

31

32

33

34

35

36

37

38

39

40

41

42

43

44

45

46

47

48

49

50

51

52

53

54

55

56

57

58

59

60

61

62

63

64

65